Ice sheet retreat and glacio-isostatic adjustment in Lützow Holm Bay, East Antarctica

Elie Verleyen[1*], Ines Tavernier[1*], Dominic A. Hodgson[2,3], Pippa Whitehouse[3], Sakae Kudoh[4], Satoshi Imura[4], Katrien Heirman[5], Michael J. Bentley[3], Steve J. Roberts [2], Marc De Batist[5], Koen Sabbe[1], Wim Vyverman[1]

[1]Lab. Protistology & Aquatic Ecology, Department of Biology, Ghent University, Campus Sterre, Krijgslaan 281 - S8, B-9000 Ghent, Belgium

[2]British Antarctic Survey, Natural Environment Research Council, High Cross, Madingley Road, Cambridge CB3 0ET, UK

[3]Durham University, Department of Geography, South Road, Durham DHI 3LE, UK

[4]National Institute of Polar Research, 10-3, Midoricho, Tachikawa, Tokyo 190-8518, Japan

[5]Renard centre of Marine Geology, Ghent University, Campus Sterre, Krijgslaan 281 - S8, B-9000 Ghent, Belgium

**equal contribution*

Author for correspondence: elie.verleyen@ugent.be

Abstract

The East Antarctic Ice Sheet (EAIS) has relatively few field data to constrain its past volume and contribution to global sea-level change since the Last Glacial Maximum. Here we provide new data on deglaciation history and glacio-isostatic uplift along a 80 km transect (from Skallen to Skarsvnes, Langhovde and the Ongul Islands) in Lützow Holm Bay, East Antarctica. Deglaciation timing was determined from the onset of organic sedimentation in lake basins combined with previously published data on exposure histories. Relative sea-level (RSL) curves were constructed based on isolation basins and evidence from raised beaches, and compared with output from two Glacial Isostatic Adjustment (GIA) models. Results showed the minimum radiocarbon age for regional deglaciation is c. 11,240 cal. yr BP on West Ongul Island with progressively younger deglaciation ages approaching the main regional ice outflow at Shirase Glacier. The geological data also revealed marked regional differences in the magnitude and timing of relative sea-level change. In Skarvsnes, a minimum marine limit of 32.7 m was inferred, which is c. 12.7 m higher than previously published evidence, and at least 15 m higher than that reported in the other three ice-free areas. RSL fall in Skarvsnes was almost an order of magnitude higher between c. 2,400 and 780 cal. yr BP (16.2 mm/yr) compared with the rate at this site from 780 cal. yr BP onwards (1.9 mm/yr) and rates in the other regions (3.6 mm/yr after c. 2,600 cal. yr BP in Skallen and 2.5 mm/yr after 5,160 cal. yr BP in the Ongul Islands). Current GIA model predictions slightly underestimate the rate of Late Holocene RSL fall at Skallen, Langhovde, and West Ongul, but provide a reasonable fit to the reconstructed minimum marine limit at these sites. GIA model predictions are unable to provide an explanation for the shape of the reconstructed RSL curve at Skarvsnes. We consider a range of possible explanations for the Skarvsnes RSL data and favour an interpretation where the anomalously high marine limit and rate of RSL fall is due to reactivation of a local fault after deglaciation in Skarsvnes.

Key-words: relative sea-level change; isolation lakes; raised beaches; Holocene; Glacial Isostatic Adjustment (GIA) Models; neotectonics

1. Introduction

Estimates of the contribution of the continental ice-sheets to past and recent global sea-level change are still relatively imprecise (Clark & Tarasov 2014). This is due to an incomplete understanding of changes in continental ice volume, including the maximum extent of glaciation, and the onset and rates of ice retreat. Some of this information can be inferred from radiocarbon dating of organic deposits that have accumulated after ice retreat (Mackintosh et al. 2014), and from changes in relative sea-level (RSL) resulting from the glacio-isostatic response of the Earth's crust to ice mass changes (Shennan et al 2015). Accurate RSL reconstructions, together with GPS-derived uplift data, can track regional changes in glacial isostatic adjustment (GIA) (Thomas et al. 2011), a process that contaminates satellite gravity measurements of present-day ice sheet mass balance (e.g., Shepherd et al. 2012, Williams et al. 2014). In regions where measurements of GIA are sparse, or where modelled estimates are not compared with geological constraints, large errors can be introduced into the GIA correction and hence the mass balance calculations (Velicogna & Wahr 2013). In Antarctica, the paucity of GIA constraints limits the accuracy of estimates of changes in the mass balance of the ice sheets derived from the Gavity Recovery and Climate Experiment (GRACE; Velicogna & Wahr

2013, Clark & Tarasov 2014). Increasing the spatial resolution of geological data on ice sheet retreat and RSL reconstructions is therefore a recognized research priority (Bentley et al. 2014).

Post Last Glacial Maximum (LGM) changes in RSL in previously glaciated regions principally reflect three processes: eustatic sea-level rise, regional GIA, and neotectonic events (Shennan et al. 2015). The latter are generally assumed to be only important in tectonically active regions (e.g., Pacific coastline of North America (Plafker 1972), the southern part of the Strait of Magellan and southernmost Tierra del Fuego (Bentley & McCulloch 2005)), and can be the dominant forcing of regional variability in RSL changes. However, post-glacial unloading and rebound can also lead to the formation or re-activation of faults in continental shields and hence tectonic activity in otherwise stable areas (e.g., Lagerbäck 1978, Risberg et al. 2005, Steffen et al. 2014). Therefore, if RSL changes are significantly influenced by neotectonic faulting, this needs to be taken into account when validating GIA models.

Of all the ice-sheets, the Antarctic ice-sheets probably have the fewest RSL field data (Bentley et al. 2014, Mackintosh et al. 2014). This has resulted in a wide range of model-based estimates of Antarctic Ice Sheet contributions to global sea-level since the LGM, varying from 35 m

(Nakada & Lambeck 1988) to 13.6 m (Argus et al. 2014), 9 ± 1.5 m (Whitehouse et al. 2012a), and even 9 to 6 m (Gomez et al. 2013). Given (i) the potential of the EAIS to raise global sea-level by up to 50 m, and (ii) indications that the melting of the EAIS likely contributed to the Eemian sea-level high stand, which was 6 to 9 m higher than today (Pingree et al. 2011), identifying those areas of the EAIS that respond to Holocene and recent climate changes is critical (Mackintosh et al. 2014).

Traditionally, RSL reconstructions in Antarctica relied on radiocarbon dating of marine fossils in raised beaches as direct evidence of former sea-level changes (e.g., Miura et al. 1998). This approach typically provides only minimum constraints on the ^{14}C age and height of former sea-levels. Another approach is based on isolation lakes, which are natural depressions in the bedrock that have been inundated by and subsequently isolated from the sea as a result of RSL fall (Verleyen et al. 2005). These basins provide more precise reconstructions of RSL changes, because their indicative meaning is known (Shennan et al. 2015). In other words, the height of their sills and their relationship with the contemporaneous sea level can be measured with more precision, which is not the case for fossils in raised beaches that might have been translocated at least by the magnitude of the tidal range, or, in the case of *in-situ* fossils (i.e., those isolated whilst still in their original living position), by the different depths at which they occur in the marine environment (Shennan et al 2015). Moreover, in isolation lakes it is possible to date the isolation event with higher precision because problems associated with the marine radiocarbon reservoir effect can be circumvented by dating organic matter in the lacustrine sediments that is deposited in equilibrium with atmospheric CO_2 (Hodgson et al. 2001, Verleyen et al. 2005). The isolation event is identified by studying markers of marine and lacustrine phases (e.g. diatoms, fossil pigments and sedimentological changes; Roberts et al. 2011). The RSL curves are then derived from studying the timing of marine-lacustrine transitions in isolation basins situated at different altitudes (Shennan et al. 2015). This approach has been applied in parts of the Antarctic Peninsula (e.g., Hall 2010, Roberts et al. 2011) and a few ice-free regions along the East Antarctic coastline (e.g., Verleyen et al. 2005; Hodgson et al. 2016).

Here, we present new RSL constraints for islands and peninsulas in the Lützow Holm Bay region (Dronning Maud Land, East Antarctica, Fig.1) based on two coastal lakes from Skarvsnes and five lakes from West Ongul Island situated at different elevations as well as new raised beach data from Skarvsnes. We combined our data with recently published records from an isolation basin on Skallen and one on Skarvsnes (Takano et al. 2012), as well as with radiocarbon dates of fossils incorporated into raised beaches on Skallen, Skarvsnes, Langhovde and West Ongul Island (Miura et al. 1998; Fig. 1). These geological constraints were subsequently compared with regional predictions of RSL evolution and high stand from two recently-developed GIA models, namely the ICE-6G_C model (Argus et al. 2014) and the W12 model (Whitehouse et al. 2012a), in order to assess the potential offset between modelling results and the near-field data.

2. Site description

Lützow Holm Bay in eastern Dronning Maud Land is part of Antarctic Drainage System 7 based on ICESat data (Fig. 1). It is the discharge point of one of the larger East Antarctic glacier systems, the Shirase Glacier, as well as a number of smaller glaciers (Miura et al. 1998). The bay includes several ice-free peninsulas and islands composed of gneisses, metabasites, and granites, together with thin beds of marble and quartzite (Tatsumi & Kizaki 1969). Different fault systems have been mapped, including one on Skarvsnes and one between West and East Ongul Island (Ishikawa et al. 1976; Fig.1), but there are no records of neotectonic activity.

West Ongul Island is the largest ice-free island in the region and it is separated from the Antarctic continent by a c. 600 m deep glacial trough (Mackintosh et al. 2014), formed by the Langhovde and Hazuki Glaciers (Miura et al. 1998). It is separated from East Ongul Island by the 40 m wide Naka-no-seto Strait. ^{14}C dates of *in situ* fossils of the marine bivalve *Laternula elliptica* and other marine macrofossils in raised beaches on the Ongul Islands fall into two age classes; pre-LGM and Holocene. It has therefore been suggested that this part of the region was ice-free during the LGM and Marine Isotope Stage (MIS) 3 (Mackintosh et al. 2014). The maximum Holocene marine limit for the region was previously estimated to be 17 m (10,590 +/- 160 ^{14}C yr BP; Miura et al. 1998).

Langhovde is one of the two main peninsulas in the region. It is situated to the South West of the Langhovde Glacier and to the North East of the Honnør Glacier. Similar to the Ongul Islands, radiocarbon dates of marine fossils in the raised beaches are either of Late Pleistocene (or older) or Holocene age. The pre-Holocene ages are only found on the Northern part, which suggests that this part was ice-free during the LGM whereas the Southern part was probably ice-covered (Mackintosh et al. 2014). The maximum Holocene marine limit has been estimated at 17 m (6,810 +/- 60 ^{14}C yr BP; Miura et al. 1998).

Skarvsnes is the second of the two largest peninsulas and is situated South of Langhovde in between glacial troughs in front of the Honnør and Telen Glaciers (Miura et al. 1998). All but one of the ^{14}C-dated fossils derived from raised marine deposits on this peninsula are of Holocene age (Miura et al. 1998), suggesting that the region was ice-covered during the LGM. This is confirmed by a recent cosmogenic isotope dating campaign, which revealed that Skarvsnes emerged from at least 350 m of ice cover between 10 and 6 ka BP (Yamane et al. 2011). The maximum Holocene marine limit at 8,440 +/- 140 ^{14}C yr BP was estimated at c. 20 m based on raised beach data (Miura et al. 1998).

Skallen is a smaller peninsula to the south-west of Skarvsnes close to the Skallen Glacier (Takano et al. 2012). It lies to the North East of the Shirase Glacier which has created a large glacial trough in Lützow Holm Bay during a succession of glacial-interglacial cycles. All the fossils sampled in raised beach deposits across the region are of Holocene age and relatively recent, suggesting that the area was ice-covered during the LGM. The maximum Holocene marine limit has been suggested to be 12 m and dated at 4,720 +/- 90 ^{14}C yr BP (Miura et al. 1998).

3. Material and methods

3.1. Geomorphological measurements, sampling of raised beaches and lake sediment coring

Three specimens of marine macrofossils (*Laternula elliptica*, and polychaete worm tubes) were sampled in raised beaches at different altitudes in Skarvsnes. Sill heights of the lakes and the raised beach deposits were surveyed using a Trimble 5700 base station GPS receiver cross-referenced to the IGS station at Syowa (code SYOG). As a test of the vertical accuracy, Geodetic Station No 39-02 was resurveyed giving an ellipsoidal height error of ± 0.97 cm. Altitudes were referenced to vertical datum WGS84 with the EGM96 geoid separation ranging from 21.14 to 22.02 m (mean 21.62 m between the ellipsoidal height and the orthometric height). Where data could not be referenced to the IGS station, spot heights of the sills of the lakes were used from previous mapping surveys (Kimura et al. 2010). A 1.5 m vertical error bar was used when developing the RSL curves to reflect the difference between low and high tide in the region.

Sediment cores were extracted from seven lakes. Five lakes were cored on West Ongul Island [Yumi Ike (WO1), Ô-Ike (WO4), Ura Ike (WO5), Higashi Ike (WO6), and Nishi Ike (WO8)] and two lakes on Skarvsnes [(Mago Ike (SK1) and Kobachi Ike (SK4)]; the codes refer to Tavernier et al. (2014) and Verleyen et al. (2012) in which more information on the limnological properties of the lakes can be found. All lakes, except Kobachi Ike were freshwater (Tavernier et al. 2014). Sediment cores were extracted using a UWITEC gravity corer for surface sediments and a Livingstone square-rod piston sampler for intermediate to basal sediments. Bedrock or glacial sediments were present at the base of all the sediment cores.

3.2. Paleolimnological analyses

To identify marine to freshwater transitions in the sediment cores, multiple biological and sedimentological proxies were analysed. Gamma ray density (GRD) and volume-specific magnetic susceptibility (MS), converted to mass-specific MS, were measured using a Bartington 1 ml MS2G sensor for those cores which were transported unsliced. The total carbon (TC) content was quantified using a Flash 2000 Organic Elemental Analyzer. Measurements were carried out by dry combustion at high temperature (left furnace: 950°C and right furnace: 840°C). Samples were all run at least twice to detect and exclude possible erroneous values. Outliers were excluded and the mean value of replicates was used. Reproducibility within and between different runs was tested using standards. Diatoms were prepared following our standardized protocols described in Tavernier et al.

(2014). Diatoms were counted using a Zeiss axiophot light microscope at a magnification of 100x10x. At least 400 valves (>2/3 intact or at least unambiguously containing the middle part of the sternum for pennate diatoms) were counted, except when concentrations were too low to reach this number. In the latter case the slides were screened in their entirity. Diatoms were grouped into freshwater, brackish and marine species based on their weighted-averaging conductivity optima as calculated in Tavernier et al. (2014). Species were considered as freshwater taxa when their WA-optimum was below 1.5 mS/cm. Species were regarded as brackish-water taxa when their WA-optimum fell between 1.5 mS/cm and 4.42 mS/cm (Tavernier et al. 2014). In the sediment cores from the brackish lake (Kobachi Ike), fossil pigments were additionally analysed, because in brackish and saline lakes identifying the marine-lacustrine transition based on fossil diatoms is sometimes complicated due to the presence of species shared between both environments. The fossil pigments were extracted and analysed following Van Heukelem & Thomas (2001). The identification of the pigments was done based on the procedures described in Tavernier et al. (2014) and pigments of unknown affinity were assigned as 'unknown' or as derivatives of the pigment with which they showed the closest match based on retention times and absorption spectra. Concentrations of individual pigments in the samples were calculated using the response factors of standard pigments. The abundance of the cyanobacteria pigments zeaxanthin, echinenone, and myxoxanthophyll is reported as a percentage of the total carotenoids (%). Myxoxanthophyll is exclusively produced by cyanobacteria and was therefore considered as the preferred marker pigment for this group, which are the dominant photoautotrophs in lacustrine microbial mat communities in East Antarctica (Verleyen et al. 2010). Hence, the presence of myxoxanthophyll was used to diagnose the onset of lacustrine conditions.

3.3. Radiocarbon dating

Lake sediment samples and marine macrofossils were dated using AMS ^{14}C by the UK Natural Environment Research Council Radiocarbon Laboratory (NERC) or the Beta Analytic Radiocarbon Dating Laboratory (Table 1). Where possible, discrete macrofossils were dated (i.e. worm tubes, sponge spicules or shells). The results are reported as conventional radiocarbon years BP with two-sigma (2σ) standard deviation error. The raised beach data were calibrated using the Marine13.14C calibration curve in CALIB (Reimer et al. 2013; Table 1). The dates from the marine sections in the sediment cores were calibrated using the mixed terrestrial SHCal13.14C and the marine13.14C calibration curve, and those of the lacustrine sediments using the terrestrial SHCal13.14C calibration curve (Hogg et al. 2013). No reservoir correction was applied to dates from lacustrine sediments, because surface-sediment dates indicate that ^{14}C in the modern lakes are in near-equilibrium with modern atmospheric CO_2 (Table 1), which is in agreement with results from other East Antarctic oases (e.g., Hodgson et al. 2001, Verleyen et al. 2011). In contrast, the AMS ^{14}C dates of the marine sediments and marine fossils in the raised beaches were corrected for the local marine reservoir effect prior to calibration using a Delta R in CALIB (Reimer et al. 2013) of 720 years, leading to a total correction of 1120 ± 100 years (see Tavernier et al. 2014 for more details regarding the reservoir correction for the region). For the ^{14}C dates of the sediments in the transition zone between the marine and lacustrine sediments in the isolation lakes calibrated using the mixed Marine and SH Atmosphere calibration curve, the percentage of marine carbon was taken into account for calculating the Delta R. This was set equal to the total relative abundance of marine diatoms following the procedures detailed in Sterken et al. (2012). The published ^{14}C dates from isolation lakes (Tanako et al. 2012) and raised beach data (Miura et al. 1998) were recalibrated following the procedures described above. Because no diatom data were available for constraining the marine to lacustrine transitions in the cores of Tanako et al. (2012), the amount of marine carbon was set at 100% in the calibration procedure for those samples that were situated in the marine sediments and the transition zone from marine to lacustrine sediments. For developing the RSL curve, calibrated median ages were used and the upper and lower limit of the calibrated ^{14}C dates defined the error bars.

3.4. Identifying RSL high stands and calculations of RSL fall

Minimum RSL high stands and their timing were defined based on the sill height of isolation lakes and ^{14}C dates of their marine sediments, or on the height of marine raised beaches and the ^{14}C ages of incorporated marine fossils. We treat these constraints as minimum marine limits because it is possible that marine sediments are present at higher altitudes, but not surveyed. The maximum RSL limits were identified based on ^{14}C dates of lacustrine sediments in glacial (always above RSL) and isolation lakes (within the range of RSL changes) and their sill heights. The rate of RSL fall was calculated by dividing the sill height of isolation lakes by the time since the lake was isolated, as determined from the calibrated ^{14}C ages of the lacustrine sediments overlying the marine sediments in these basins.

3.5. Glacial Isostatic Adjustment modelling

A GIA model was used to calculate predicted RSL curves for the four ice-free regions. Each of the four peninsula and island sub-areas are small enough (max 16 km across) that the variation in predicted RSL within them would be smaller than the uncertainty in the observations. Therefore, a single RSL prediction is provided for each island and peninsula area, and the sea-level indicators for that location may be combined into a single RSL curve. In contrast, the distance between the outcrops across the whole study area is large enough for there to be a gradient in GIA. This, combined with the differing distances of the islands and peninsulas from former ice loading centres, justifies the need for a different RSL prediction for each outcrop. The GIA model calculates the solid Earth response to ice and ocean loading through time, and the corresponding change in the shape of the geoid (Kendall et al. 2005). The Earth is represented by a three-layer, spherically-symmetric, viscoelastic Maxwell body, while the ice loading history is defined by either the W12 (Whitehouse et al. 2012a) or the ICE-6G_C (Argus et al. 2014) model. The W12 model is combined with the northern hemisphere component of the ICE-5G model (Peltier 2004) such that both ice models define the global change in ice loading throughout the last glacial cycle. Ocean loading is determined by solving the sea-level equation

(Farrell and Clark 1976). In combination with the W12 model we use the optimum Earth model of Whitehouse et al. (2012b), which comprises a 120 km-thick lithosphere, an upper mantle of viscosity 10^{21} Pa s, and a lower mantle of viscosity 10^{22} Pa s. In contrast, the ICE-6G_C ice loading history should be combined with the VM5a Earth model (Peltier et al. 2015). The VM5a model does not take a uniform viscosity value in the lower mantle (Peltier et al. 2015), so we use an approximation of this model that has a 96 km-thick lithosphere, an upper mantle of viscosity 0.5 x 10^{21} Pa s, and a lower mantle of viscosity 3 x 10^{21} Pa s. From here onwards we use the terms W12 model and ICE-6G_C model to refer to the combination of the ice and Earth model in each case. RSL predictions are extracted from the models at the four study sites.

4. Results

4.1. Initial ice sheet retreat

The start of biogenic sedimentation in the lacustrine sediments of glacial lakes and marine sedimentation in isolation basins provides minimum ages of initial ice sheet retreat over the terrestrial and nearshore marine environment respectively (cf. Hodgson et al. 2001; Table 1). The latter were combined with ^{14}C dates of marine fossils in raised beaches. In

Skallen, Skarvsnes, and Langhovde no glacial lakes were cored. In the most southerly peninsula, Skallen, the oldest marine ^{14}C date was derived from a raised beach at 7 m a.s.l. and is 7,580 cal. yr BP, while the oldest date of marine sediments in the Skallen Ike basin (9.6 m a.s.l.) is 5,810 cal. yr BP (Miura et al. 1998; Fig.2a). In Skarvsnes, polychaete tubes in a raised beach at 18 m a.s.l. are 8,670 cal. yr BP old (Fig. 2b) while the oldest date in a marine sediment core sequence comes from the isolation lake Kobachi Ike (28 m a.s.l.), and is 7,430 cal. yr BP old (Fig. 2b; Table 1). The oldest Holocene marine ^{14}C date in Langhovde is 10,390 cal. yr BP and was derived from a shell of *Adamussium colbecki* situated in a raised beach at 6 m a.s.l. (Miura et al. 1998; Fig. 2c). The basal age of the freshwater sediment cores from Nishi Ike (23 m a.s.l.) in the Ongul Islands is almost 1000 years older (i.e., 11,240 cal. yr BP), which agrees well with the oldest post-LGM date of a marine fossil (shell fragment) in raised beaches at 17 m a.s.l. on these islands (10,810 cal. yr BP; Miura et al. 1998; Fig.2d).

4.2. Regional differences in relative sea-level changes

The analyses of fossil diatoms and the sedimentology in all cores, in combination with fossil pigments in Kobachi Ike, revealed that a total of 26 radiocarbon dates from the lake sediment cores were of marine or mixed marine-lacustrine origin, while 39 were deposited in a lacustrine environment (See supplementary material for a description and an interpretation of the proxy records; Fig.S1-S4; Table 1). Combined with the ^{14}C dates of the raised beaches, these ages show that the RSL curves of Skallen, Langhovde and the Ongul Islands were broadly similar, but differed markedly with the one from Skarvsnes (Fig. 2a-d). In Skallen, the minimum recorded sea-level high stand is 12 m at c. 4,020 cal. yr BP based on the raised beach data. RSL fall equalled no more than 3.7 mm/yr on average and was higher than 2.9 mm/yr during the past c. 2,600 cal. yr BP as revealed by the first ^{14}C date in the lacustrine and the last deposited marine sediments respectively in Lake Skallen. In Langhovde, no lake records are available preventing the calculation of a robust rate of RSL fall. Based on the raised beach data alone, the minimum marine limit was estimated to be 17 m at 6,530 cal yr BP. In West Ongul Island, the maximum marine limit was below 17 m after 6,288 cal. yr BP as indicated by the absence of ^{14}C dates with a marine origin in Ura Ike, and never exceeded 23 m during the past 11,240 cal. yr BP based on the presence of exclusively lacustrine sediments in the Nishi Ike basin. The raised beach data revealed that the minimum marine limit on the islands is 17 m at 10,813 cal. yr BP. RSL fall equalled on average 2.5 mm/yr during the past

c. 5,160 cal. yr BP and 2.3 mm/yr during the past c. 4,360 cal. yr BP based on the isolation of Yumi Ike. In Skarvsnes, the minimum RSL high stand is 32.7 m based on a new radiocarbon date of a marine macrofossil (shell) of 5,410 ± 40 ^{14}C yr old (5,265 – 4,653 cal. yr BP) preserved in marine sediments in the upper sill of Kobachi Ike (Table 1). The other macrofossils for which new ^{14}C dates are available are from *L. elliptica* and *polychaete* tubes preserved in raised beaches at a height of 8.6 m a.s.l. and they are respectively 4,730 ± 40 and 6,800 ± 40 ^{14}C yr old (Table 1). In Skarvsnes, RSL fall was more rapid during the past 2,410 cal. yr BP than in the Ongul Islands and Skallen and equalled on average 11.6 mm/yr. The dominance of brackish diatoms at 93 cm and the presence of the cyanobacterial pigment myxoxanthophyll (from 115 cm onwards) in the Kobachi Ike sediment core are used to infer lacustrine conditions (Fig. S4 and supplementary text) and hence lake isolation in this calculation. Between c. 2,410 (first lacustrine ^{14}C date in Kobachi Ike (28 m a.s.l.)) and 780 cal. yr BP (first lacustrine ^{14}C date in Mago Ike; 1.5 m.a.s.l.), the mean rate of RSL fall was 16.2 mm/yr, but this dropped to a rate of 1.9 mm/yr from c. 780 cal. yr BP onwards, which is of the same order as that recorded in the other two regions. The inference of the start of freshwater conditions during the Late Holocene in

Kobachi Ike also shows that RSL did not fall below 28 m a.s.l. until 2,410 cal. yr BP (Fig.2b).

4.3. Ice sheet model outputs and comparison with geological constraints

The maximum RSL high stand in the output of the W12 model is consistently lower and occurs slightly later compared with the ICE-6G_C model, although the difference between the two models decreases with distance from the Shirase Glacier (Fig.2a-d). Along the South to North gradient away from the Shirase Glacier (i.e., between Skallen and the Ongul Islands), the maximum RSL high stand varied between c. 29 and 20.3 m and between c. 14.3 and 12.4 m in the output of the ICE-6G_C and W12 models, respectively. The output of the W12 model provides a reasonable fit to the highest radiocarbon date of a marine raised beach sample in Skallen, although this was not necessarily the marine limit. This model also agreed well with the geological constraints on the RSL high stand in the Ongul Islands, but underestimates the RSL high stand in Langhovde and particularly in Skarvsnes. The rate of RSL fall during the Late Holocene is underestimated by this model in all four regions and particularly in Skarvsnes. With the exception of the Ongul Islands, this is also more or less the case with the output from the ICE-6G_C model which underestimates RSL fall in the three other regions. The high stand is is predicted by the ICE-6G_C model to lie above the elevation of the highest marine fossils in Skallen and Langhovde, although these fossils were not necessarily sampled at the maximum marine limit. The ICE-6G_C model provides a good fit to the raised beach and lake data in the Ongul Islands and gets closer to matching the highest marine fossils at Skarsvnes. However, in the latter region the timing of the modelled RSL high stand is too early compared with the geological constraints from Kobachi Ike.

5. Discussion

5.1. Initial ice sheet retreat since the Last Glacial Maximum

The ^{14}C dates in the bottom sediments of the lakes indicate an Early Holocene ice sheet retreat over the study sites, which started later near the Shirase Glacier (7,580 cal yr BP in Skallen) than in the regions further to the North (Langhovde and the Ongul Islands). The oldest ^{14}C date (c. 11,240 cal. yr BP, see Table 1) was obtained in lacustrine sediments overlying glacial sediments in a core from Nishi Ike, a glacial lake in West Ongul Island. This suggests (scenario 1) that the region was ice-covered during the LGM as a result of the expansion of the EAIS and that it became gradually ice-free during the Early Holocene. This is in general agreement with cosmogenic isotope data from Skarvsnes and a large number of the currently ice-free regions in East Antarctica, such as Schirmacher Oasis, the Vestfold Hills, and the Windmill Islands (see Hall 2009 and Mackintosh et al. 2014 for a review). However, scenario 1 contradicts with the alternative interpretation (scenario 2) which involves ice-free conditions during the LGM based on the published raised beaches from the region in which well-preserved *in situ* shells of *L. elliptica* predate the LGM (Miura et al. 1998). These *in situ* fossils suggest that the nearshore zone of the Ongul islands was ice-free during MIS3. One hypothesis to explain this discrepancy is that marine habitats were ice-free during the LGM leading to the *in situ* preservation of fossils, while terrestrial habitats were ice-free yet covered with permanent snow banks on ice-covered lakes such as Niski Ike. This snow cover would have prevented light penetration and hence primary production in the lakes (cf. Gore 1997). The fact that the islands remained exposed and escaped glacial overriding might be due to an expanding glacier flowing around, but not over, the Ongul Islands and its shallow marine habitats (raised beaches), through the 600 m deep Fuji Submarine Valley. Another possibility, which is in agreement with scenario 1, is that the islands were ice-covered during the LGM but the shells remained preserved under a more or less inactive ice-sheet buttressed on the Ongul

Islands, with the major ice flow lines diverted into the deep glacial troughs between the islands and the continent. A similar process likely resulted in the preservation of Eemian sediments in Progress Lake in the Larsemann Hills, which became ice-free during the Late-Holocene (Hodgson et al. 2006).

Deglaciation of the coastal zone near Skarvsnes seems to have started somewhere around c. 7430 cal. yr BP, as evidenced by the oldest radiocarbon date obtained from the marine sediments in Kobachi Ike. This timing is in agreement with that obtained from the radiocarbon dates in the raised beaches (Miura et al. 1998, Fig.2b); where apart from two dates, none is older than c. 8000 cal. yr BP. Moreover, our estimate also corresponds to a cosmogenic isotope dating study which places the deglaciation of Skarvsnes between 10 and 6 ka BP (Yamane et al. 2011). More precisely, the time of deglaciation of the Kobachi Ike basin agrees well with that obtained for nearby Mount Suribati. This timing slightly postdates the start of deglaciation in scenario 1 in the Ongul Islands further to the North. Clearly, if the Ongul Islands were ice-free during MIS3 (scenario 2), the differences in glacial history between these islands and the other ice-free regions in Lützow Holm Bay would be even more pronounced. The regional differences in deglaciation are furthermore supported by geomorphological evidence and the degree of weathering of the bedrock. Indeed, rocks in the northernmost part of Sôya Coast are deeply weathered, whereas those in the southern part of the coast (i.e. Skarvsnes and Skallen) are relatively unweathered and intensively striated. Such pronounced differences in the deglaciation history between regions only 60-80 km apart from each other have also been observed elsewhere such as in Prydz Bay (Hodgson et al. 2001, 2016). The deglaciation of Skarvsnes and Skallen is also clearly later than most other East Antarctic regions (Mackintosh et al. 2014). However, these findings corroborate recent evidence from regions along the Rayner Glacier (Enderby Land) to the east of Lützow Holm Bay that became ice-free between 9 and 6 ka (White & Fink 2014). It is clear that additional geomorphological research and radiometric dating of landforms and lake sediments is needed to fully resolve the deglaciation history of Lützow Holm Bay (Mackintosh et al. 2014).

5.2. Geological constraints on changes in relative sea-level

Our most significant finding is the striking difference in the RSL high stands and rates of RSL fall between Skallen, Langhovde and the Ongul islands on the one hand, and Skarvsnes on the other (Fig.2a-d). In Skallen, the raised beach data suggest that the RSL high stand was situated at least at 12 m. It is possible that the limit was actually higher, but this needs to be confirmed by additional dating of bottom sediments of glacial lakes (i.e. those that have remained above the Holocene marine limit) and additional surveying of raised beaches in the region at higher altitudes. In the Ongul Islands, RSL was always below 23 m a.s.l. during the Holocene as indicated by the presence of exclusively lacustrine sediments in the glacial lake Nishi Ike between c. 11,240 cal. yr BP until present. The absence of raised beaches 6 m below the sill height of this lake and the absence of marine sediments in the two other glacial lakes (Ura Ike at 17 m a.s.l. and Higashi Ike at 18 m a.s.l.) suggests that the marine limit in the Ongul Islands is probably even lower (i.e., at 17 m a.s.l.). In Langhovde, the raised beach data suggest that the marine limit is similarly at 17 m a.s.l. Taken together, these marine limits are close to previous estimates based on raised beach data alone (Miura et al. 1998). By contrast, the minimum marine limit in Skarvsnes is at least 9 m higher than the maximum marine limit in the Ongul Islands, and 12 m higher than previous estimates for the peninsula based on raised beach data alone (Miura et al. 1998). The rate of RSL fall is also different between Skarvsnes and the other three regions. In Skarvsnes, RSL fall was on average 11.6 mm/yr during the past 2,400 years. This far exceeds the rates in Skallen and the Ongul Islands, which equalled 3.6-2.9 mm/yr during the past c. 2,600 cal. yr BP and 2.5 mm/yr during the past c. 5,160 cal. yr BP, respectively. This difference is mainly related to the rapid RSL fall between 2,400 cal yr BP (isolation of Kobachi Ike) and 780 cal. yr BP (isolation of Mago Ike) in Skarvsnes. These contrasts in the RSL curves in the different regions are potentially underlain by three different, non-mutually exclusive processes, namely regional variation in (i) the timing of deglaciation, (ii) local ice-sheet volume and (iii) neotectonic processes. The first process is less likely, given the relatively small regional differences in the timing of the start of deglaciation between Skallen and Skarvsnes. Also, the second process can be expected to be negligible, because RSL changes typically reflect regional changes in ice thickness rather than local small-scale differences. GIA could only produce such a spatial contrast in RSL rate if the upper mantle were locally very weak (e.g. Simms et al. 2012) and there had been a short-lived, localised period of significant ice loss in Skarvsnes. There is no evidence for either condition being upheld. We therefore speculate that the third hypothesis is the most likely, given the small distance between the different sites, the presence of a mapped fault system on Skarvsnes and other faults in the bay (Ishikawa et al. 1976; Fig.1), and the well-known tendency for post-glacial crustal stress to result in fault rupture in some locations (Bentley & McCulloch 2005, Steffen et al. 2014). A reactivation of this fault system in response to glacial unloading, could explain the sudden difference in RSL fall in Skarvsnes between c. 2400 and 780 cal. yr BP (rate of 16.2 mm/yr) compared with a rate of 1.9 mm/yr from c. 780 cal. yr BP onwards. Short-term tectonic activities along existing fault lines was also hypothesised to explain regional patterns in RSL fall along the Baltic coast of Sweden (Risberg et al. 2005). Similarly, in the Strait of Magellan (South Chile) there is evidence for post-glacial fault movement of at least 30 m, based on the proxy record from a bog near Puerto del Hambre and the regional history of proglacial lakes (Bentley & McCulloch 2005). On account of the differences in RSL changes between the islands and peninsulas in Lützow Holm Bay we consider that the three similar records (Skallen, Langhovde, Ongul) can be used to constrain GIA models, but that Skarvsnes should be considered an outlier. This could be confirmed by further geological and geomorphological data from either side of the fault lines.

5.3. Comparison between geological constraints and monitoring and modelling results

The rate of RSL fall in Skallen and the Ongul Islands, which equalled 3.6 mm/yr on average during the past c. 2,600 cal. yr BP and 2.5 mm/yr on average during the past c. 5,160 cal. yr BP respectively, is comparable with data obtained from short-term GPS measurements of local crustal deformation between 1999-2003 in Skallen (3.00 +/- 1.9 mm/yr; 69.6710 S, 39.3987 E) and between 1998 and 2004 (2.56 +/- 0.24 mm/yr; Ohzono et al. 2006) in West Ongul Island (69.0070 S, 39.5833 E). In Skarvsnes the rate of RSL fall is 1.9 mm/yr from c. 780 cal. yr BP onwards, which is in relatively good agreement with the uplift rate measured using GPS monitoring stations in the region (1.12 +/- 1.46 mm/yr, 69.4738 S, 39.6071 E; Ohzono et al. 2006). This confirms the robustness of our approach. However, ignoring the anomalous curve before c. 780 cal yr BP at Skarvsnes, the shape and high stand of the RSL curves based on the geological data are not always in agreement with GIA modelling results. For example, the ICE-6G_C model provides a reasonable fit to the recent rate of RSL fall at Skallen but this rate is under-predicted by the W12 model. Both models under-predict the recent rate of RSL fall at Langhovde, but fit the data reasonably well in the Ongul Islands. The greater magnitude of the high stand predicted by the ICE-6G_C model at all four locations is due to a combination of two factors: (i) The ICE-6G_C model includes a greater magnitude of regional ice loss since the LGM compared with the W12 model, and (ii) it uses a weaker value for the upper and lower mantle viscosity. The lack of robust, independent constraints on either of these factors makes this an underdetermined problem. Regional RSL data therefore play a vital role in reducing the uncertainty on ice history and Earth rheology around Antarctica.

6. Conclusions

The minimum age for deglaciation of the Lützow Holm Bay region is c. 11,240 cal. yr BP on West Ongul Island with progressively younger deglaciation ages approaching the main regional ice outflow at Shirase Glacier. It remains unclear whether parts of the region were ice-free during the LGM, or alternatively covered by permanent snow banks or an inactive ice sheet. Of most significance is the difference in (i) the Holocene RSL high stand and (ii) the shape of the RSL curves in Skarvsnes compared with those in the Ongul Islands, Langhovde and Skallen. We attribute these regional differences to neotectonic events in response to ice sheet retreat. Current GIA model predictions give a reasonable fit to the reconstructed RSL curves at Skallen, Langhovde, and West Ongul, but they are unable to explain the pattern recorded at Skarvsnes. Our results call for a critical reassessment of existing RSL curves along the East Antarctic coastal margin.

7. Acknowledgements

We thank the Belgian Science Policy Office (HOLANT project), the UK Natural Environment Research Council (British Antarctic Survey and Radiocarbon Laboratory), Maaike Vancauwenberghe and the Japanese Antarctic Research Expedition 48 for financial and logistical support. EV was a post-doctoral research fellow with the Fund for Scientific Research Flanders during part of the research. IT was funded by the Institute for the Promotion of Innovation by Science and Technology in Flanders. PLW is a recipient of a NERC Independent Research Fellowship (NE/K009958/1). Ilse Daveloose (Ghent University) is thanked for the help with the HPLC analysis of the fossil pigments. Laura Gerrish (BAS, UK) is thanked for providing figure 1.

References

Argus, D.F., Peltier, W.R., Drummond, R. & Moore, A.W. (2014) The Antarctica component of postglacial rebound model ICE-6G_C (VM5a) based on GPS positioning, exposure age dating of ice thicknesses, and relative sea level histories. Geophysical Journal International, 198, 537-563.

Bentley MJ, and McCulloch (2005) Impact of neotectonics on the record of glacier and sea level fluctuations, Strait of Magellan, southern Chile. Geografiska Annaler, 87A, 393-402.

Bentley, M.J., Cofaigh, C.O., Anderson, J.B., Conway, H., Davies, B., Graham, A.G.C., Hillenbrand, C.D., Hodgson, D.A., Jamieson, S.S.R., Larter, R.D., Mackintosh, A., Smith, J.A., Verleyen, E., Ackert, R.P., Bart, P.J., Berg, S., Brunstein, D., Canals, M., Colhoun, E.A., Crosta, X., Dickens, W.A., Domack, E., Dowdeswell, J.A., Dunbar, R., Ehrmann, W., Evans, J., Favier, V., Fink, D., Fogwill, C.J., Glasser, N.F., Gohl, K., Golledge, N.R., Goodwin, I., Gore, D.B., Greenwood, S.L., Hall, B.L., Hall, K., Hedding, D.W., Hein, A.S., Hocking, E.P., Jakobsson, M., Johnson, J.S., Jomelli, V., Jones, R.S., Klages, J.P., Kristoffersen, Y., Kuhn, G., Leventer, A., Licht, K., Lilly, K., Lindow, J., Livingstone, S.J., Masse, G., McGlone, M.S., McKay, R.M., Melles, M., Miura, H., Mulvaney, R., Nel, W., Nitsche, F.O., O'Brien, P.E., Post, A.L., Roberts, S.J., Saunders, K.M., Selkirk, P.M., Simms, A.R., Spiegel, C., Stolldorf, T.D., Sugden, D.E., van der Putten, N., van

Ommen, T., Verfaillie, D., Vyverman, W., Wagner, B., White, D.A., Witus, A.E., Zwartz, D. & Consortium, R. (2014) A community-based geological reconstruction of Antarctic Ice Sheet deglaciation since the Last Glacial Maximum. Quaternary Science Reviews, 100, 1-9.

Clark, P.U. & Tarasov, L. (2014) Closing the sea level budget at the Last Glacial Maximum. Proceedings of the National Academy of Sciences of the United States of America, 111, 15861-15862.

Farrell W.E., Clark J.A. (1976). Post-glacial sea level. Geophysical Journal of the Astronomical Society 46, 647-667.

Gomez N., Pollard D., and Mitrovica J.X. (2014) A 3-D coupled ice sheet – sea level model applied to Antarctica through the last 40 ky. Earth and Planetary Science Letters 384, 88-99.

Gore DB (1997) Blanketing snow and ice; constraints on radiocarbon dating deglaciation in East Antarctic oases. Antarctic Science, 9, 336-346.

Hall BL (2009) Holocene glacial history of Antarctica and the sub-Antarctic islands. Quaternary Science Reviews, 28, 2213-2230.

Hall BL (2010) Holocene relative sea-level changes and ice fluctuations in the South Shetland Islands. Global and Planetary Change, 74, 15-26.

Hodgson DA, Noon PE, Vyverman W, Bryant CL, Gore DB, Appleby P, Gilmour M, Verleyen E, Sabbe K, Jones VJ, Ellis-Evans JC, Wood PB (2001) Were the Larsemann Hills ice-free through the Last Glacial Maximum? Antarctic Science, 13, 440-454.

Hodgson DA, Verleyen E, Sabbe K, Squier AH, Keely BJ, Leng MJ, Saunders KM, Vyverman W (2005) Late Quaternary climate-driven environmental change in the Larsemann Hills, East Antarctica, multi-proxy evidence from a lake sediment core. Quaternary Research, 64, 83–99.

Hodgson DA, Verleyen E, Squier AH, Sabbe K, Keely BJ, Saunders KM, Vyverman W (2006) Interglacial environments of coastal east Antarctica: comparison of MIS 1 (Holocene) and MIS 5e (Last Interglacial) lake-sediment records. Quaternary Science Reviews, 25, 179-197.

Hodgson, D.A., Whitehouse, P.L., De Cort, G., Berg, S., Verleyen, E., Tavernier, I., Roberts, S.J., Vyverman, W., Sabbe, K. & O'Brien, P. (2016) Rapid early Holocene sea-level rise in Prydz Bay, East

Antarctica. Global and Planetary Change, 139, 128-140.

Hogg, A.G., Hua, Q., Blackwell, P.G., Niu, M., Buck, C.E., Guilderson, T.P., Heaton, T.J., Palmer, J.G., Reimer, P.J., Reimer, R.W., Turney, C.S.M. & Zimmerman, S.R.H. (2013) SHCAL13 Southern Hemisphere calibration, 0-50,000 years CAL BP. Radiocarbon, 55, 1889-1903.

Ishikawa T, Tatsumi K, Kizaki K, Yanai H, Ando T, Kikuchi Y, Yoshida Y (1976) Explanatory text of geological map of Langhovde, Antarctica. *Antarctic Geological Map Seriers Sheet 5, Langhovde, National Institute of Polar Research,* 12.

Kendall, R. A., Mitrovica, J. X., and Milne, G. A. (2005) On post-glacial sea level – II. Numerical formulation and comparative results on spherically symmetric models, Geophysical Journal International 161, 679–706.

Kimura S, Ban S, Imura S, Kudoh S, Matsuzaki M (2010) Limnological characteristics of vertical structures in the lakes of Syowa Oasis, East Antarctica. Polar Science, 3, 262-271.

Lagerbäck, 1978. Neotectonic structures in northern Sweden. Geologiska Foreningen i Stockholm Forhan-dlingar Volume: 100 Pages: 263-269

Lambeck K., Rouby H., Purcell A. Sun Y.Y. (2014). Sea level and global ice volumes from the Last Glacial Maximum to the Holocene. Proceedings of the National Academies of Science of the United States of America, 111, 15296-15303.

Mackintosh, A.N., Verleyen, E., O'Brien, P.E., White, D.A., Jones, R.S., McKay, R., Dunbar, R., Gore, D.B., Fink, D., Post, A.L., Miura, H., Leventer, A., Goodwin, I., Hodgson, D.A., Lilly, K., Crosta, X., Golledge, N.R., Wagner, B., Berg, S., van Ommen, T., Zwartz, D., Roberts, S.J., Vyverman, W. & Masse, G. (2014) Retreat history of the East Antarctic Ice Sheet since the Last Glacial Maximum. Quaternary Science Reviews, 100, 10-30.

Miura H, Maemoku H, Igarashi A, Moriwaki K (1998) Late Quaternary raised beach deposits and radiocarbon dates of marine fossils around Lützow Holm Bay. Special map series of National Institute of Polar Research, 6, pp. 46.

Nakada, M. & Lambeck, K. (1988) The melting history of the Late

Pleistocene ice sheet. Nature, 333, 36-40.

Ohzono M, Tabei T, Doi K, Shibuya K, Sagiya T (2006) Crustal movement of Antarctica and Syowa Station based on GPS measurements. Earth Planets Space, 58, 795-804.

Peltier W.R. (2004) Global glacial isostasy and the surface of the ice-age earth: The ice-5G (VM2) model and grace. Annual Review of Earth and Planetary Sciences, 32, 111-149.

Peltier W.R., Argus D.F., Drummond R. (2015) Space geodesy constrains ice age terminal deglaciation: The global ICE-6G_C (VM5a) model. Journal of Geophysical Research – Solid Earth, 120, 450-487.

Pingree, K., Lurie, M. & Hughes, T. (2011) Is the East Antarctic ice sheet stable? Quaternary Research, 75, 417-429.

Plafker G. (1972) Alaskan earthquake of 1964 and Chilean earthquake of 1960 – implications for arc tectonics. Journal of Geophysical Research, 77, 901-926.

Reimer, P.J., Bard, E., Bayliss, A., Beck, J.W., Blackwell, P.G., Ramsey, C.B., Buck, C.E., Cheng, H., Edwards, R.L., Friedrich, M., Grootes, P.M., Guilderson, T.P., Haflidason, H., Hajdas, I., Hatte, C., Heaton, T.J., Hoffmann, D.L., Hogg, A.G., Hughen, K.A., Kaiser, K.F., Kromer, B., Manning, S.W., Niu, M., Reimer, R.W., Richards, D.A., Scott, E.M., Southon, J.R., Staff, R.A., Turney, C.S.M. & van der Plicht, J. (2013) INTCAL13 and MARINE13 radiocarbon age calibration curves 0-50,000 years cal BP. Radiocarbon, 55, 1869-1887.

Risberg J, Alm G, Goslar T (2005) Variable isostatic uplift patters during the Holocene in southeast Sweden, based on high-resolution AMS radiocarbon datings of lake isolations. The Holocene, 15, 847-857.

Roberts SJ, Hodgson DA, Sterken M, Whitehouse PL, Verleyen E, Vyverman W, Sabbe K, Balbo A, Bentley MJ, Morteton S (2011) Geological constraints on glacio-isostatic adjustment models of relative sea-level change during deglaciation of Prince Gustav Channel, Antarctic Peninsula. Quaternary Science Reviews, 30, 3603-3617.

Shennan I, Long AJ, Horton BP (2015) Handbook of sea-level research. American Geophysical Union, 600 pp.

Shepherd, A., Ivins, E.R., Geruo, A., Barletta, V.R., Bentley, M.J., Bettadpur, S., Briggs, K.H., Bromwich, D.H., Forsberg, R., Galin, N., Horwath, M., Jacobs, S., Joughin, I., King, M.A., Lenaerts, J.T.M., Li, J.L., Ligtenberg, S.R.M., Luckman, A., Luthcke, S.B., McMillan, M., Meister, R., Milne, G., Mouginot, J., Muir, A., Nicolas, J.P., Paden, J., Payne, A.J., Pritchard, H., Rignot, E., Rott, H., Sorensen, L.S., Scambos, T.A., Scheuchl, B., Schrama, E.J.O., Smith, B., Sundal, A.V., van Angelen, J.H., van de Berg, W.J., van den Broeke, M.R., Vaughan, D.G., Velicogna, I., Wahr, J., Whitehouse, P.L., Wingham, D.J., Yi, D.H., Young, D. & Zwally, H.J. (2012) A Reconciled Estimate of Ice-Sheet Mass Balance. Science, 338, 1183-1189.

Simms A.R., Ivins E.R., DeWitr R., Kouremenos P., Simkins L.M. (2012). Timing of the most recent Neoglacial advance and retreat in the South Shetland Islands, Antarctic Peninsula: insights from raised beaches and Holocene uplift rates. Quaternary Science Reviews, 47, 41-55.

Steffen, R., Wu, P., Steffen, H. & Eaton, D.W. (2014) On the implementation of faults in finite-element glacial isostatic adjustment models. Computers & Geosciences, 62, 150-159.

Sterken, M., Roberts, S.J., Hodgson, D.A., Vyverman, W., Balbo, A.L., Sabbe, K., Moreton, S.G. & Verleyen, E. (2012) Holocene glacial and climate history of Prince Gustav Channel, northeastern Antarctic

Peninsula. Quaternary Science Reviews, 31, 93-111.

Takano Y, Tyler JJ, Kojima H, Yokoyama Y, Tanabe Y, Sato T, Ogawa NO, Ohkouchi N, Fukui M (2012) Holocene lake development and glacial-isostatic uplift at Lake Skallen and Lake Oyako, Lützow Holm Bay, East Antarctica, based on biogeochemical facies and molecular signatures. *Applied Geochemistry*, doi: http://dx.doi.org/10.1016/j.apgeochem.2012.08.009

Tatsumi T. and Kizaki K. (1969) Geology of the Lützow Holm Bay region and the 'Yamato Mountains' (Queen Fabiola Mountains). Geologic maps of Antarctica. Edited by C. Craddock, New York, American Geographic Society, Plate 10.

Tavernier, I., Verleyen, E., Hodgson, D.A., Heirman, K., Roberts, S.J., Imura, S., Kudoh, S., Sabbe, K., De Batist, M. & Vyverman, W. (2014) Absence of a Medieval Climate Anomaly, Little Ice Age and twentieth century warming in Skarvsnes, Lutzow Holm Bay, East Antarctica. Antarctic Science, 26, 585-598.

Thomas, I. D., King, M. A., Bentley, M. J., Whitehouse, P. L., Penna, N. T., Williams, S. D. P., Riva, R. E. M., Lavallee, D. A., Clarke, P. J., King, E. C., Hindmarsh, R. C. A. and Koivula, H. (2011). Widespread low rates of Antarctic glacial isostatic adjustment revealed by GPS observations. Geophysical Research Letters 38: article number L22302.

Van Heukelem L, and Thomas CS (2001) Computer-assisted high-performance liquid chromatography method development with applications to the isolation and analysis of phytoplankton pigments. Journal of Chromatography A, 910, 31-49.

Velicogna, I. & Wahr, J. (2013) Time-variable gravity observations of ice sheet mass balance: Precision and limitations of the GRACE satellite data. Geophysical Research Letters, 40, 3055-3063.

Verleyen E, Hodgson DA, Milne GA, Sabbe K, Vyverman W (2005) Relative sea-level history from the Lambert glacier region, East Antarctica, and its relation to deglaciation and Holocene glacier readvance. Quaternary Research, 63, 45-52.

Verleyen E, Sabbe K, Hodgson DA, Grubisic S, Taton A, Cousin S, Wilmotte A, De Wever A, Van der Gucht K, Vyverman W (2010) Structuring effects of climate-related environmental factors on Antarctic microbial mat communities. Aquatic Microbial Ecology, 59, 11-24.

Verleyen, E., Hodgson, D.A., Sabbe, K., Cremer, H., Emslie, S.D., Gibson, J., Hall, B., Imura, S., Kudoh, S., Marshall, G.J., McMinn, A., Melles, M., Newman, L., Roberts, D., Roberts, S.J., Singh, S.M., Sterken, M., Tavernier, I., Verkulich, S., Van de Vyver, E., Van Nieuwenhuyze, W., Wagner, B. & Vyverman, W. (2011) Post-glacial regional climate variability along the East Antarctic coastal margin-Evidence from shallow marine and coastal terrestrial records. Earth-Science Reviews, 104, 199-212.

Verleyen E, Hodgson DA, Gibson J, Imura S, Kaup E, Kudoh S, De Wever A, Hoshino T, McMinn A, Obbels D, Roberts D, Roberts SJ, Sabbe K, Souffreau C, Tavernier I, Van Nieuwenhuyze W, Van Ranst E, Vindevogel N, Vyverman W (2012) Chemical limnology in coastal East Antarctic lakes: monitoring future climate change in centres of endemism and biodiversity. Antarctic Science, 24, 23-33.

White, D.A. & Fink, D. (2014) Late Quaternary glacial history constrains glacio-isostatic rebound in Enderby Land, East Antarctica. Journal of Geophysical Research-Earth Surface, 119, 401-413.

Whitehouse PL, Bentley MJ, Le Brocq AM (2012a) A deglacial model for Antarctica; geological constraints and glaciological modeling as a bias for a new model of Antarctic glacial isostatic adjustment. Quaternary Science Reviews, 32, 1-24.

Whitehouse P.L., Bentley M.J.B. Milne G.A., King M.A., Thomas I.D. (2012b) A new glacial isostatic adjustment model for Antarctica: calibrated and tested using observations of relative sea-level change and present-day uplift rates. Geophysical Journal International, 190, 1464–1482.

Williams, S.D.P., Moore, P., King, M.A. & Whitehouse, P.L. (2014) Revisiting GRACE Antarctic ice mass trends and accelerations considering autocorrelation. Earth and Planetary Science Letters, 385, 12-21.

Yamane M, Yokoyama Y, Miura H, Maemoku H, Iwasaki S, Matsuzaki H (2011) The last deglacial history of Lützow Holm Bay, East Antarctica. Journal of Quaternary Science, 26, 3-6.

Figure captions

Fig. 1: Overview map of Antarctica with an indication of the study area, and a map of Lützow Holm Bay with an indication of the study sites: the Ongul Islands, Langhovde, Skarvsnes and Skallen. The inset shows the location of the lakes used for developing the RSL curves in Fig.2: Yumi Ike (WO1, 10 m a.s.l.), Ô-Ike (WO4, 13 m a.s.l.), Ura Ike (WO5, 17 m a.s.l.), Higashi Ike (WO6, 18 m a.s.l.), Nishi Ike (WO8, 23 m a.s.l.), Mago Ike (SK1, 1.5 m a.s.l.) and Kobachi Ike (SK4, 28 m a.s.l.). The lake codes refer to Tavernier et al. (2014) and Verleyen et al. (2012). The data for Lake Oyako (2.4 m a.s.l.) and Lake Skallen (9.6 m a.s.l.) are based on Takano et al. (2012).

Fig.2: Relative sea level curves for (a) Skallen, (b) Skarvsnes, (c) Langhovde and (d) the Ongul Islands; the order of the regions is in increasing distance from the Shirase Glacier. The plots show the height above present sea level (a.s.l.; grey stippled horizontal line) of the median calibrated ^{14}C dates of the marine fossils in the raised beaches (blue circles), the marine sediments in the isolation lakes (blue squares) and the lacustrine sediments in the glacial and isolation lakes (red squares). The dark blue circles in fig.2b denote the new raised beach data. The red

symbols represent the maximum upper limit of the RSL curve, while the blue symbols are the minimum upper limit. The vertical error bar was set at 0.75 m corresponding to the maximum tidal range in the region that exceeds the error of the measurements of the heights of the deposits. The horizontal error bars correspond to the minimum and maximum ranges of the calibrated ^{14}C dates. The green line is the output of the W12 model (Whitehouse et al. 2012a), and the black line is the output from our approximation of the ICE-6G_C model (Argus et al., 2014). The full blue line is a hand-drawn approximation of the minimum RSL based on the available ^{14}C dates of marine sediments in isolation basins or marine raised beaches.

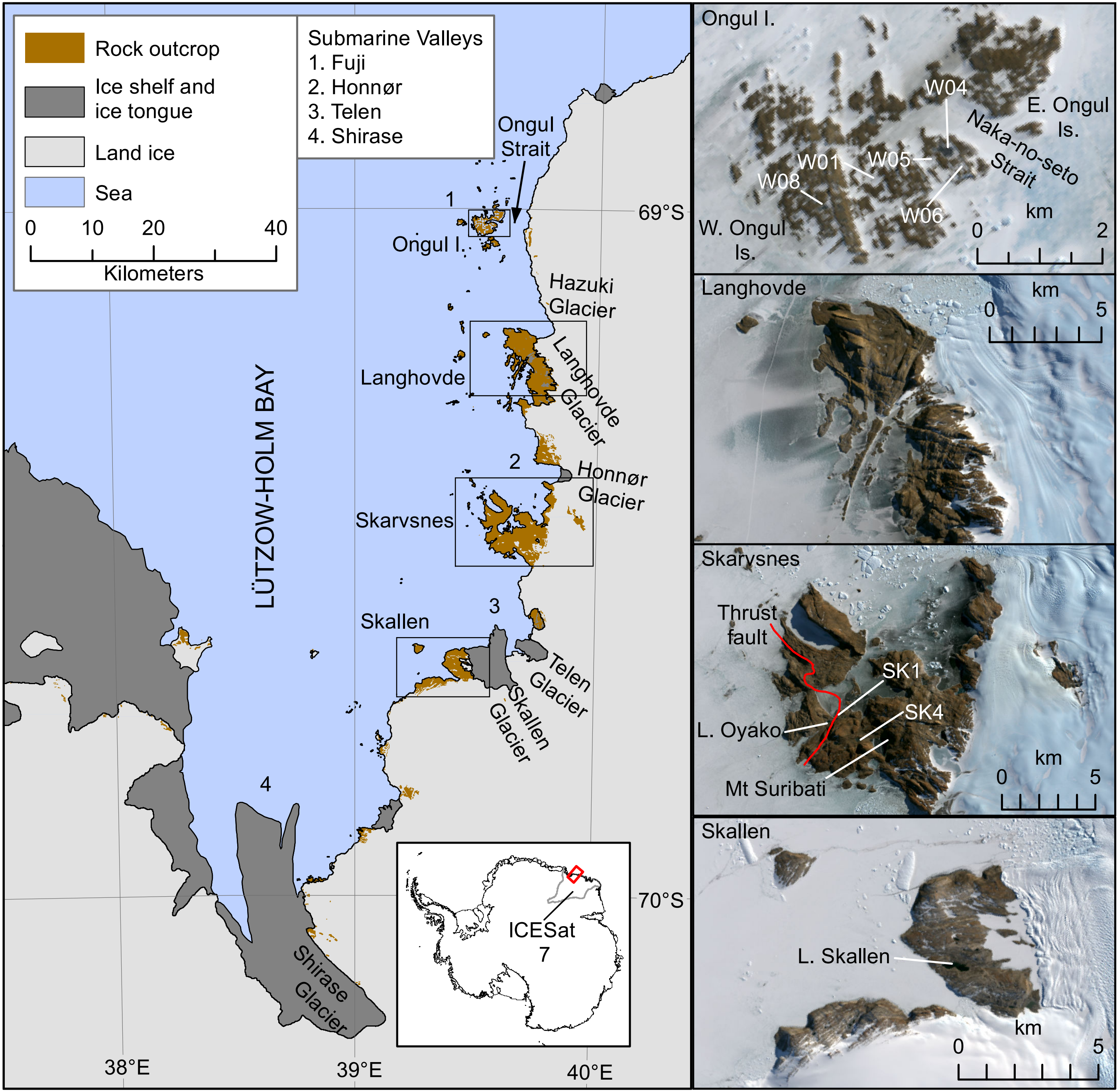

Rock outcrop
Ice shelf and ice tongue
Land ice
Sea
0 10 20 40
Kilometers
Submarine Valleys
1. Fuji
2. Honnør
3. Telen
4. Shirase
Ongul Strait
1
Ongul I.
69°S
Hazuki Glacier
Langhovde
Langhovde Glacier
2
Honnør Glacier
Skarvsnes
LÜTZOW-HOLM BAY
3
Skallen
Telen Glacier
Skallen Glacier
4
Shirase Glacier
ICESat 7
70°S
38°E
39°E
40°E
Ongul I.
W04
E. Ongul Is.
Naka-no-seto Strait
W01
W05
W08
W06
W. Ongul Is.
km
0 2
Langhovde
km
0 5
Skarvsnes
Thrust fault
SK1
SK4
L. Oyako
Mt Suribati
km
0 5
Skallen
L. Skallen
km
0 5

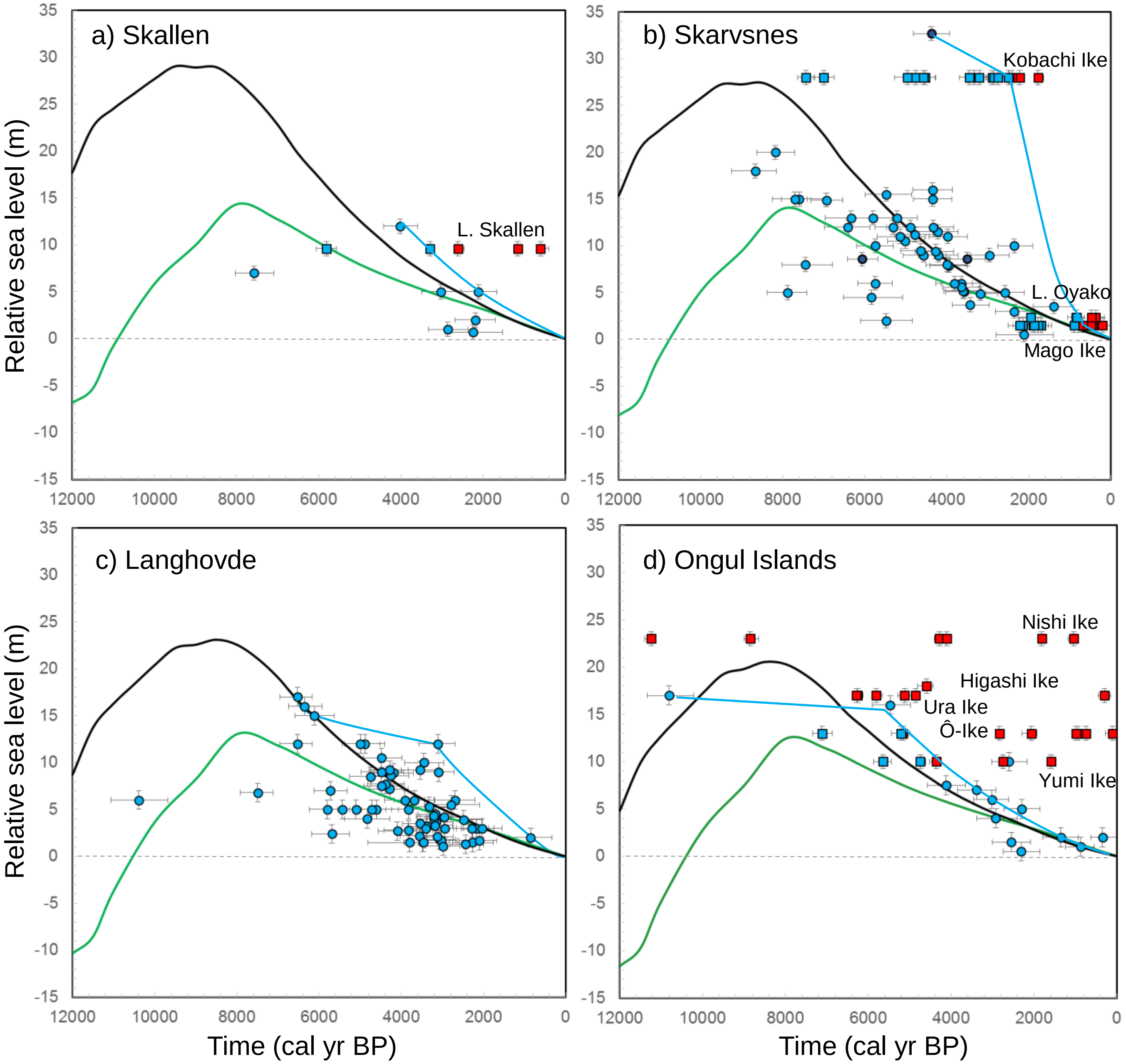

a) Skallen
L. Skallen
b) Skarvsnes
Kobachi Ike
L. Oyako
Mago Ike
c) Langhovde
d) Ongul Islands
Nishi Ike
Higashi Ike
Ura Ike
Ô-Ike
Yumi Ike
Relative sea level (m)
Time (cal yr BP)

Supplementary text

Description of the paleolimnological proxy analyses of the sediment cores

Isolation lakes

<u>Yumi Ike, West Ongul Island - 10 m above sea-level (a.s.l.)</u>

In the Yumi Ike cores (Fig. S1) a marine zone (WO1-I), a lacustrine freshwater zone (WO1-III), and a transition zone (WO1-II) in between could be identified based on the proxy data. Between 74 and 54 cm core depth, marine diatoms dominated and the total carbon (TC) concentration was relatively low. Mass-specific magnetic susceptibility (MS) values decreased towards the end of this zone whereas gamma ray density (GRD) remained relatively stable. The transition zone between 54 and 46 cm contained a mixture of brackish-water and marine diatom species. The TC concentration remained low. MS values slightly increased, whereas GRD remained stable. From 46 cm until the surface sediments, freshwater diatoms were dominant and brackish and marine diatoms occasionally occurred, likely as a result of sea spray and/or the visit of the lake by marine birds or mammals. The TC concentration was more variable than in the other two zones. MS values further increased to reach a maximum at 37.2 cm, decreased until 14 cm, and rose again. GRD remained relatively stable to become slightly higher in the upper 5 cm of the sediments.

<u>Ô–Ike, West Ongul Island - 13 m a.s.l.</u>

Similar to Yumi Ike, three main zones were identified in the Ô-Ike sediment cores (Fig. S2), namely a marine zone (WO4 I), a lacustrine freshwater zone (WO4 III) and a very short transition zone in between (WO4 II). In zone WO4 I, between 176 and 160 cm, TC concentrations were low, while GRD and MS were relatively high. The latter decreased towards the end of this zone. This zone was dominated by marine diatoms, while freshwater species were absent. Between 160 and 158 cm, TC concentrations were still low. This zone was dominated by marine and brackish water diatoms. GRD and MS decreased throughout this zone. Between 158 cm and the top of the core, the TC concentration was relatively high. WO4 III was dominated by freshwater diatoms. GRD remained relatively stable and was lower in this zone compared with zone WO I and WOII until 86.6 cm, above which no measurements were available. MS was low and stable throughout this zone.

Mago Ike, Skarvsness - 1.5 m a.s.l.

Again, three main zones were identified (Fig. S3), namely a marine zone (SK1 I), a lacustrine freshwater zone (SK1 III) and a transition zone in between (SK1 II). Between 254 and 143 cm, the TC concentration was very low. GRD and MS were relatively high and the latter increased towards the end of the zone. Marine diatoms dominated, while brackish-water and particularly freshwater species were only present in low abundances. Between 143 cm and 123 cm TC started to increase. GRD decreased in SK1 II while MS reached a maximum and subsequently dropped sharply. The relative abundance of brackish-water diatoms increased towards the upper part of this zone, while the percentage of marine diatoms decreased. Between 123 cm and the top of the core, TC concentration was relatively high, while GRD and MS were relatively low. This zone was dominated by freshwater diatoms; some brackish-water and marine diatoms occasionally occurred at the beginning of this zone.

Kobachi Ike, Skarvsness - 28 m a.s.l.

The evolution of Kobachi Ike is more complex and the delineation between the different zones was less straight forward compared with the other isolation basins. This is due to the gradual change in the abundance of brackish water versus marine diatoms and the presence of the latter in the entire core, resulting in a slow species turnover in the sedimentary communities. This gradual change is likely related to the volume and shape of the lake basin in relation to the amount of meltwater entering the lake. In the other study lakes, the meltwater input is high compared with the volume of the basin, leading to a flushing of the trapped marine water after lake isolation, which in turn resulted in the establishment of freshwater conditions and the colonization by freshwater organisms. By contrast, in Kobachi Ike, the relatively low amount of meltwater entering the lake only slowly diluted the marine water. Moreover, due to the relatively deep water column, the lake is chemically stratified as brackish conditions prevail in the bottom waters (specific conductance below 2.4 m depth equaled 11.4 mS/cm at the time of sampling), while low salinity waters (specific conductance of 5.0 mS/cm) were present in the upper 2.4 m of the water column. This freshwater lens is likely derived from meltwater input from the catchment and/or lake ice (Kimura et al. 2010). The salinity-driven stratified conditions appear to be strong enough to prevent mixing of the bottom water with meltwater. Furthermore, this situation also provides a mechanism for the passage of large fluxes of meltwater without significantly affecting the salinity of the lake as freshwater can pass through the epilimnion and leave the lake via an outflow stream (which was not active during sampling) without diluting the brackish water stored in the hypolimnion. Hence, instead of the relatively rapid dilution of the lake water in the smaller polymictic freshwater lakes and the subsequent changes in the diatom communities, marine species could probably survive in saline conditions in Kobachi Ike for hundreds of years. This was for example also the case in the saline lakes of the Vestfold Hills (Roberts and McMinn 1999), which are still dominated by marine taxa (Verleyen et al. 2003). Based on the diatoms, pigments and sedimentological changes, the sediment cores could be subdivided in three main zones (Fig. S4), namely a zone consisting of glacial sediments (SK4 I), and a marine zone (SK4 II), which gradually evolved towards a lacustrine zone (SK4 III). Between 280 and 245 cm, the total chlorophyll and total carotenoid concentrations as well as the relative abundance of cyanobacterial carotenoids, MS and total diatom concentration were low. From 260 cm onwards, zone SK4 I was further characterized by relatively high TOC concentrations. Myxoxanthophyll, a cyanobacterial marker pigment was absent throughout this zone. Between 245 and 115 cm, the TOC concentrations, and the total chlorophyll and carotenoid concentrations were low. Myxoxanthophyll was almost completely absent in zone SK4 II. This zone was furthermore characterized by relatively high MS values. Marine diatoms were dominant, but brackish-water species became more abundant from c. 165 cm depth. It follows that lake isolation may have started in this zone already. In zone SK4 III, between 115 cm and the top of the core, the TOC, chlorophyll and carotenoid concentrations were relatively high. Myxoxanthophyll became a subdominant pigment which marks the presence of cyanobacteria. Benthic cyanobacterial mats are abundant in East Antarctic lakes (Verleyen et al. 2010) and Kobachi Ike today (Obbels et al. unpubl. results), but largely absent from the Southern Ocean (Fukuda et al. 1998). However, we considered the zone between 115 cm and 93 cm as a transition zone, because marine diatoms remained dominant in this part of the core. Hence, the ^{14}C dates at 115 and 107 cm were calibrated using the mixed marine and SH curve. We interpreted the dominance of the diatom communities by brackish water species as the start of the establishment of fully lacustrine conditions (at 93 cm depth). However, spores from marine *Chaetoceros* species remained an important member of the assemblages in some samples. These spores can be *in situ* produced, although it is also possible that they were transported to the lake through sea spray, or alternatively that they were washed-in from raised beach deposits within the catchment area. The start of the dominance of the brackish water diatoms also coincided with a decrease in magnetic susceptibility (MS) that further gradually declined from 82 cm. This decrease in MS also suggests a complete isolation of the lake, which was for example similarly observed in Maritime Antarctic lakes and related to differences in the sedimentary infill of the basins during marine versus lacustrine conditions (Watcham et al. 2011). During the latter, mainly local minerals are transported to the basin while during marine conditions sediments from elsewhere might be transported to the site via ice bergs and redistributed sea ice containing wind-blown particles. Hence, we considered the start of the dominance by brackish water diatoms at 93 cm depth as marking the establishment of full lacustrine conditions.

Glacial lakes

All the samples analysed in the glacial lakes on West Ongul Island Ura Ike (17 m a.s.l.), Higashi Ike (18 m a.s.l.) and Nishi Ike (23 m a.s.l.) were dominated by freshwater lacustrine diatoms. The basal ages of the Higashi Ike and Nishi Ike sediment cores are c. 4520 or 4560 and c. 11,240 cal. yr BP, respectively. In Ura Ike, age reversals occurred (Table S1) between 73 and 59 cm, making it difficult to determine the age of the bottom sediments. However, the oldest ^{14}C date obtained suggests that Ura Ike is at least c. 6290 cal. yr BP old. Combined, these data suggest that these basins were situated above the marine limit throughout the entire Holocene and probably originated from beneath the ice-sheet or permanent snow fields during the Early- to Mid-Holocene.

Reference list

Fukuda, R., Ogawa, H., Nagata, T. & Koike, I. (1998) Direct determination of carbon and nitrogen contents of natural bacterial assemblages in marine environments. Applied and Environmental Microbiology, 64: 3352-3358.

Kimura S, Ban S, Imura S, Kudoh S, Matsuzaki M (2010) Limnological characteristics of vertical structures in the lakes of Syowa Oasis, East Antarctica. Polar Science, 3: 262-271.

Roberts, D. & McMinn, A. (1999) A diatom-based palaeosalinity history of Ace Lake, Vestfold Hills, Antarctica. Holocene, 9: 401-408.

Verleyen, E., Hodgson, D.A., Vyverman, W., Roberts, D., McMinn, A., Vanhoutte, K. & Sabbe, K. (2003) Modelling diatom responses to climate induced fluctuations in the moisture balance in continental Antarctic lakes. Journal of Paleolimnology, 30: 195-215.

Verleyen, E., Sabbe, K., Hodgson, D.A., Grubisic, S., Taton, A., Cousin, S., Wilmotte, A., De Wever, A., Van der Gucht, K. & Vyverman, W. (2010) Structuring effects of climate-related environmental factors on Antarctic microbial mat communities. Aquatic Microbial Ecology, 59: 11-24.

Watcham, E.P., Bentley, M.J., Hodgson, D.A., Roberts, S.J., Fretwell, P.T., Lloyd, J.M., Larter, R.D., Whitehouse, P.L., Leng, M.J., Monien, P. & Moreton, S.G. (2011) A new Holocene relative sea level curve for the South Shetland Islands, Antarctica. Quaternary Science Reviews, 30: 3152-3170.

Captions to the supplementary figures

Fig.S1: Summary diagram of the Yumi Ike (WO1 – 10 m a.s.l.) sediment core showing the lithology, total carbon content (TC), mass specific magnetic susceptibility (MS), gamma ray density (GRD), and the percentage of lacustrine freshwater, brackish and marine diatoms. The dates are median calibrated ^{14}C ages. Dates in blue were calibrated using the mixed SH marine-terrestrial calibration curve and those in black using the SH Cal13 terrestrial calibration curve.

Fig.S2: Summary diagram of the Ô Ike (WO4 – 13 m a.s.l.) sediment core showing the lithology and legend, total carbon content (TC), mass specific magnetic susceptibility (MS), gamma ray density (GRD), and the percentage of lacustrine freshwater, brackish and marine diatoms. GRD and MS were only measured on cores transported intact to the laboratory (between c. 176 and 86 cm depth). The color code for the dates is as in fig.S1.

Fig.S3: Summary diagram of the Mago Ike (SK1 – 1.5 m a.s.l.) sediment core showing the lithology and legend, total carbon content (TC), gamma ray density (GRD), mass specific magnetic susceptibility (MS), and the percentage of lacustrine freshwater, brackish and marine diatoms. The color code for the dates is as in fig.S1. For depths for which two dates are available, the date of the bulk material is on the right and the date of macrofossils on the left.

Fig.S4: Summary diagram of the Kobachi Ike (SK4 – 28 m a.s.l.) sediment core showing the lithology and legend, total carbon content (TC), the total chlorophyll and carotenoid concentration, the relative abundance of cyanobacteria marker pigments, and the percentage of myxoxanthophyll (%); a pigment exclusively produced by cyanobacteria. Also shown are the gamma ray density (GRD), mass specific magnetic susceptibility (MS), and the percentage of lacustrine freshwater, brackish and marine diatoms. The grey horizontal bar represents a zone of low diatom production. The green line represents the interpreted start of full lacustrine conditions based on the dominance of brackish water diatoms. The color code for the dates is as in fig.S1.

Supplementary tables

Table S1: Conventional and calibrated radiocarbon dates of the lake sediment core and raised beach data. Dates indicated with an asterisk were corrected for the regional marine reservoir effect (1120 years). For samples situated in the marine to lacustrine transition zone (see supplementary material), the relative abundance of marine diatoms was used to assess the percentage of marine carbon present. CRA = Conventional Radiocarbon Age.

depth (cm)	Dated material	Publication code	$\delta^{13}C_{VPDB}$ ‰ ± 0.1	CRA (yr BP ± 1σ)	Median age CALIB (yr BP)	age ranges CALIB (yr BP)	Rel. area under probability distribution
Ô-Ike							
0	microbial mat	SUERC - 18342	-14.2	149 ± 35	107	1-153	0.730
						175-176	0.001
						210-276	0.268
26	microbial mat	Beta - 279334	-12.8	880 ± 40	745	674-803	0.976
						872-882	0.015
						890-897	0.009
51	microbial mat	Beta - 279335	-21.2	1080 ± 40	944	808-886	0.124
						901-994	0.773
						1015-1055	0.103
89	microbial mat	Beta - 261170	-	2130 ± 40	2066	1932-1970	0.049
						1991-2157	0.919
						2267-2296	0.032
92	microbial mat	Beta - 261171	-	1130 ± 40	991	929-1061	1
104	microbial mat	Beta - 261172	-15.1	4570 ± 40	5163	4988-4993	0.004
						5039-5317	0.996
132	microbial mat	Beta - 322269	-13.1	2790 ± 30	2837	2763-2928	1
155*	bulk matrix	SUERC - 18067	-23.2	4583 ± 36	5164	5046-5205	0.624
						5210-5318	0.376
157*	bulk matrix	SUERC - 18068	-23.6	4856 ± 38	5206	5043-5325	0.971
						5414-5440	0.029
168*	bulk matrix	Beta - 261174		7240 ± 50	7116	6866-7352	1
171	bulk matrix			insufficient CO_2			
Yumi Ike							
0	microbial mat	SUERC - 18338	-14.6	modern			
14	microbial mat	Beta - 322266	-16.2	1730 ± 30	1594	1533-1629	0.715
						1645-1700	0.285
28	microbial mat	Beta - 322267	-8.3	2660 ± 30	2751	2548-2552	0.002
						2621-2627	0.004
						2706-2796	0.975
						2822-2842	0.018
39	microbial mat	SUERC - 18056	-21.6	3970 ± 35	4361	4240-4445	0.934
						4474-4477	0.003
						4480-4514	0.063
52	microbial mat	Beta - 322268	-21.7	4460 ± 30	4744	4617-4769	0.612
						4780-4854	0.388
73*	bulk matrix	SUERC - 18066	-18.5	5893 ± 38	5649	5449-5880	1
Nishi Ike							
0	microbial mat	SUERC - 18345	-13.7	modern			
10	microbial mat	Beta - 322270	-11	1200 ± 30	1047	968-1111	0.882
						1136-1174	0.118
18	microbial mat	Beta - 322271	-12.8	1920 ± 30	1818	1734-1890	1
40	microbial mat	Beta - 322272	-16.2	3900 ± 30	4284	4155-4209	0.328
						4221-4297	0.172
						4218-4411	0.828
40	microbial mat	Beta - 327120	-	3790 ± 30	4107	3984-4182	0.908
						4197-4232	0.092
55	microbial mat	SUERC - 18071	-21.2	8019 ± 40	8850	8649-8677	0.042
						8684-8686	0.001
						8694-8998	0.957
60	microbial mat	Beta - 322273	-23.4	9870 ± 60	11240	11129-11398	1
71	microbial mat			insufficient CO_2			
Ura Ike							
0	microbial mat	SUERC - 18343	-28.4	281 ± 37	298	150-217	0.287
						272-331	0.500
						365-443	0.213
59	microbial mat	SUERC - 18070	-31.1	5090 ± 38	5810	5663-5691	0.051
						5708-5906	0.949
60	microbial mat	SUERC - 18069	-30	5500 ± 38	6254	6130-6137	0.004
						6181-6320	0.981
						6373-6390	0.015
70	microbial mat	SUERC - 18058	-30.7	5528 ± 37	6288	6205-6352	0.914
						6366-6396	0.086
73	microbial mat	Beta - 327121	-29.9	4340 ± 30	4860	4827-4964	1
73	microbial mat	Beta - 326318	-30.6	4500 ± 30	5123	4893-4898	0.003
						4919-4926	0.005
						4960-5290	0.991
Higashi Ike							
0	microbial mat	SUERC - 18344	-13.9	modern			
51	microbial mat	Beta - 326319	-15.3	4130 ± 30	4596	4441-4484	0.078
						4511-4660	0.639
						4663-4709	0.089
						4755-4813	0.194
64	microbial mat			insufficient CO_2			
Kobachi Ike							
0	microbial mat	SUERC – 18336	-25.8	modern			1
57	microbial mat	SUERC – 18051	-25.4	1875 ± 35	1774	1633-1642	0.010
						1701-1840	0.960
						1850-1872	0.030
70	microbial mat	SUERC – 18063	-25.5	2234 ± 35	2223	2098-2133	0.082
						2143-2324	0.918
80	microbial mat	Beta – 261164	-24.4	2410 ± 40	2412	2314-2502	0.887
						2593-2614	0.024
107*	microbial mat	SUERC – 18352	-24.5	3527 ± 38	2895	2738-3084	0.987
						3087-3105	0.013
115*	microbial mat	Beta – 326312	-23.4	3490 ± 30	2854	2720-3048	1
136*	Bulk matrix	Beta – 326313	-23.7	3980 ± 30	3335	3118-3556	1
157*	Bulk matrix	SUERC – 18353	-23.6	4176 ± 35	3452	3208-3688	1
170*	Bulk matrix	Beta – 326314	-22.6	4940 ± 30	4528	4287-4801	1
184*	Bulk matrix	SUERC – 18354	-22.2	5282 ± 37	4755	4445-5037	1
207*	Bulk matrix	Beta – 326315	-22.4	5120 ± 40	4564	4273-4827	1
231*	Bulk matrix	Beta – 311995	-19.6	3700 ± 30	2756	2453-3018	1
233*	Bulk matrix	SUERC – 18355	-17.9	3466 ± 36	2480	2209-2215	0.002
						2240-2731	0.998
233b*	Bulk matrix	Beta – 326316	-18.9	3480 ± 30	2496	2248-2742	1
240*	Bulk matrix			insufficient CO_2			
245*	Bulk matrix	Beta – 311996	-17.3	4080 ± 30	3209	2923-3456	1
260*	Bulk matrix	Beta – 326317	-18.3	5420 ± 40	4958	4681-5275	1
274*	Bulk matrix	Beta – 261166	-	7650 ± 60	7434	7226-7642	1
279*	Bulk matrix	SUERC – 18356	-21.5	7219 ± 41	7001	6740-7242	1
Mago Ike							
30	microbial mat	BETA-306508	-14.6	230 ± 30	197	1-2	0.002
						74-81	0.008
						108-111	0.003
						142-227	0.704
						252-306	0.283
56	microbial mat	SUERC-19466	-16.7	413 ± 37	438	323-415	0.459
						426-502	0.541
77.5	microbial mat	BETA-306509	-14.0	450 ± 30	481	333-363	0.132
						444-516	0.868
91.5	microbial mat	BETA-306510	-15.8	460 ± 30	490	336-357	0.077
						448-521	0.923
111.4	microbial mat	SUERC-19467	-14.5	788 ± 37	685	573-587	0.032
						646-735	0.968
113.4	microbial mat	SUERC-19468	-14.5*	919 ± 37	780	722-906	1
122.1*	Bulk matrix	BETA-261161	-	1300 ± 40	896	778-982	1
168*	Bulk matrix	SUERC-18048	-17.5	2785 ± 35	1698	1448-1453	0.001642
						1456-1941	0.998358
201*	Bulk matrix	SUERC-18049	-16.2	2993 ± 37	1898	16-2152	1
227*	Bulk matrix	SUERC-18050	-17.3	3208 ± 35	2144	1868-2384	1
227*	sponge spicule	SUERC-18348	-0.3	2902 ± 35	1774	1523-2031	1
253*	Bulk matrix	SUERC-18062	-17.2	3274 ± 37	2220	1928-2510	1
253*	worm tube	SUERC-18349	-0.1	2974 ± 35	1862	1595-2122	1
Beaches							
SK3ML*	carbonate shell	Beta-261163	0.9	5410 ± 40	4913	4823 - 5028	1
SK4MLLAT*	carbonate shell	Beta-261167	0.2	4730 ± 40	4021	3889 - 4144	1
SK4 ML POLY*	polychaete tube	Beta-261168	0.2	6800 ± 40	6504	6401 - 6617	1

Fig.S1

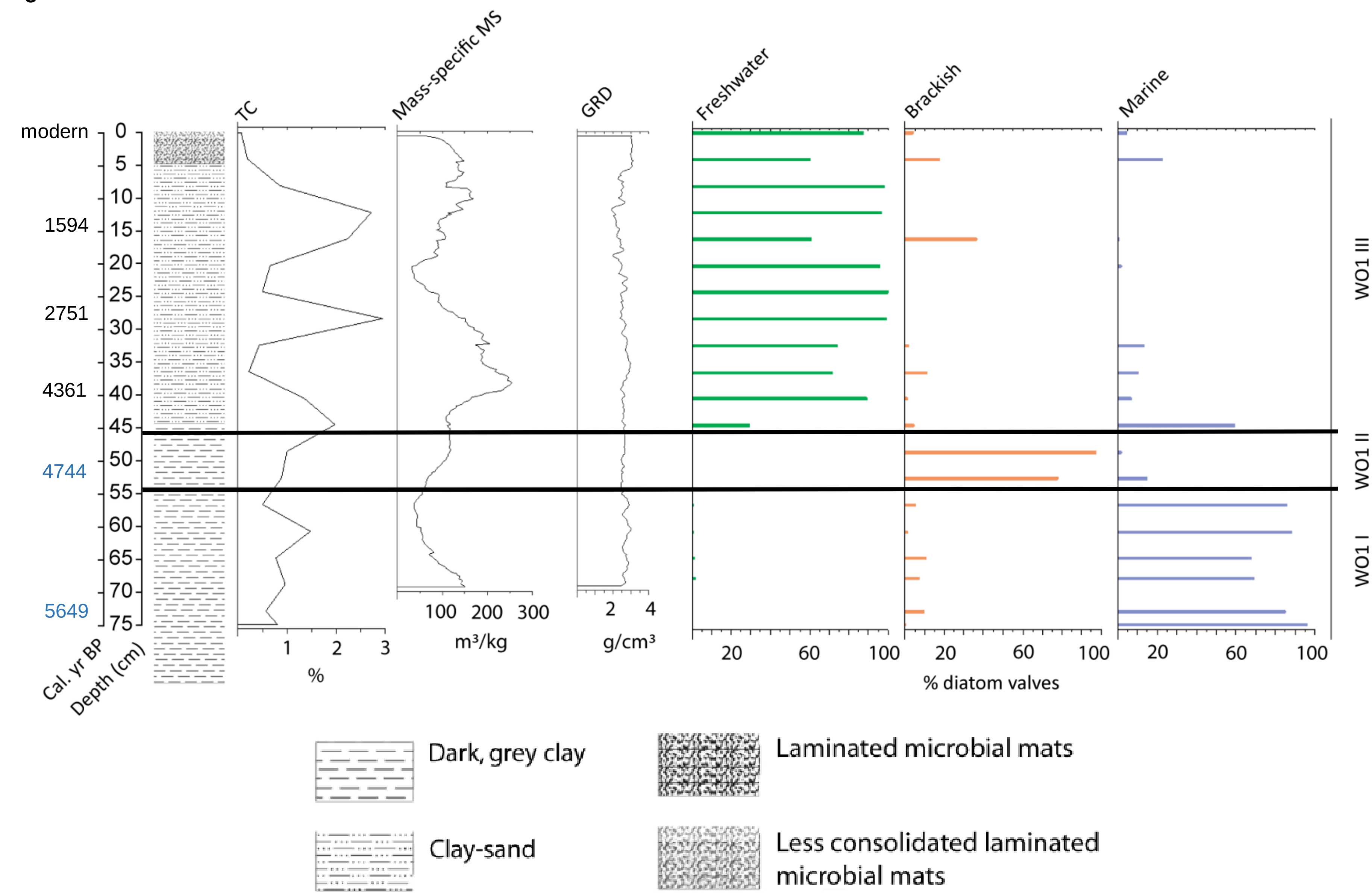

TC
Mass-specific MS
GRD
Freshwater
Brackish
Marine
modern
1594
2751
4361
4744
5649
Cal. yr BP
Depth (cm)
0
5
10
15
20
25
30
35
40
45
50
55
60
65
70
75
1 2 3
%
100 200 300
m³/kg
2 4
g/cm³
20 60 100
% diatom valves
WO1 III
WO1 II
WO1 I
Dark, grey clay
Clay-sand
Laminated microbial mats
Less consolidated laminated microbial mats

Fig.S2

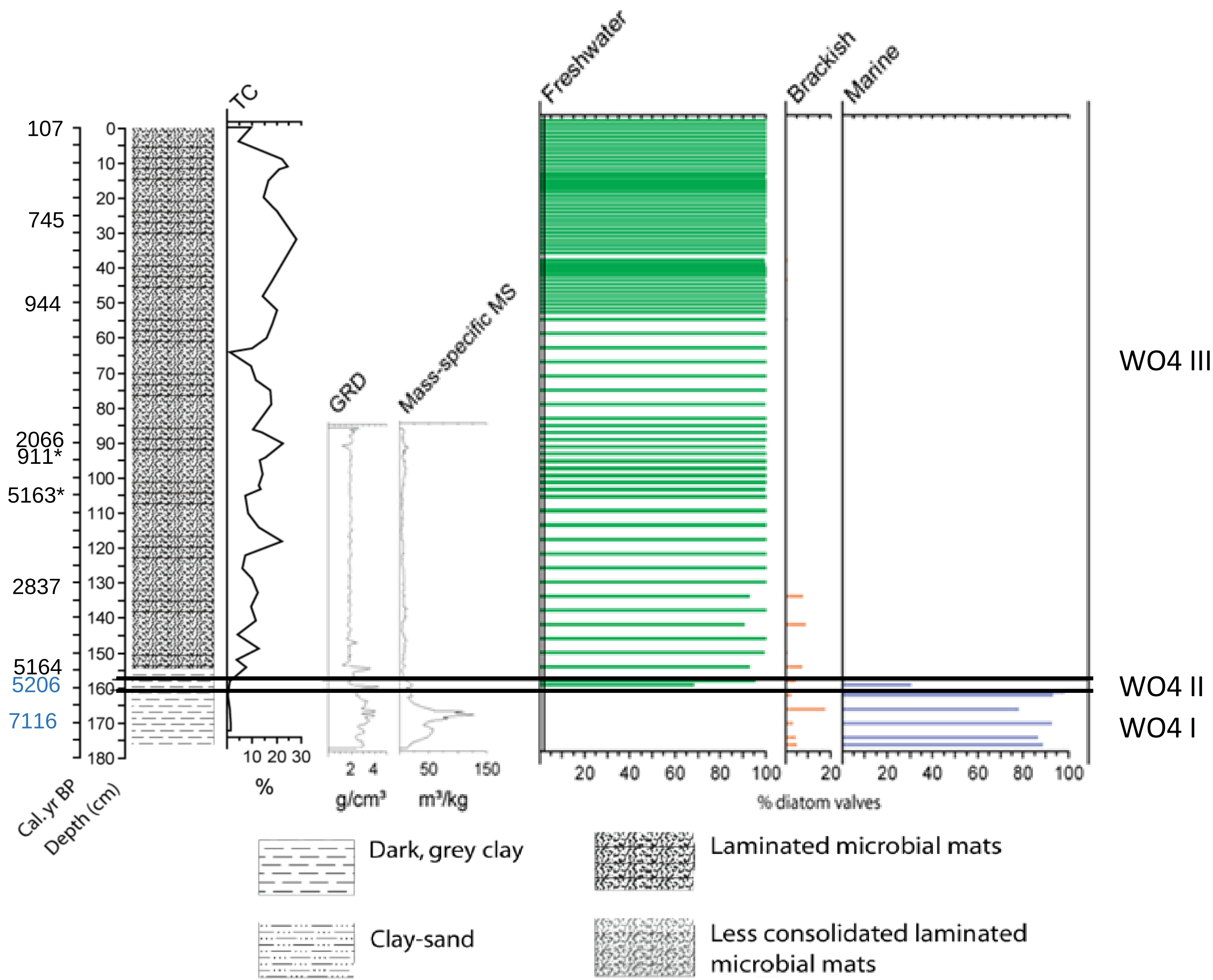
TC
GRD
Mass-specific MS
Freshwater
Brackish
Marine
107
745
944
2066
911*
5163*
2837
5164
5206
7116
Cal.yr BP
Depth (cm)
%
g/cm³
m³/kg
% diatom valves
WO4 III
WO4 II
WO4 I
Dark, grey clay
Clay-sand
Laminated microbial mats
Less consolidated laminated microbial mats

Fig.S3

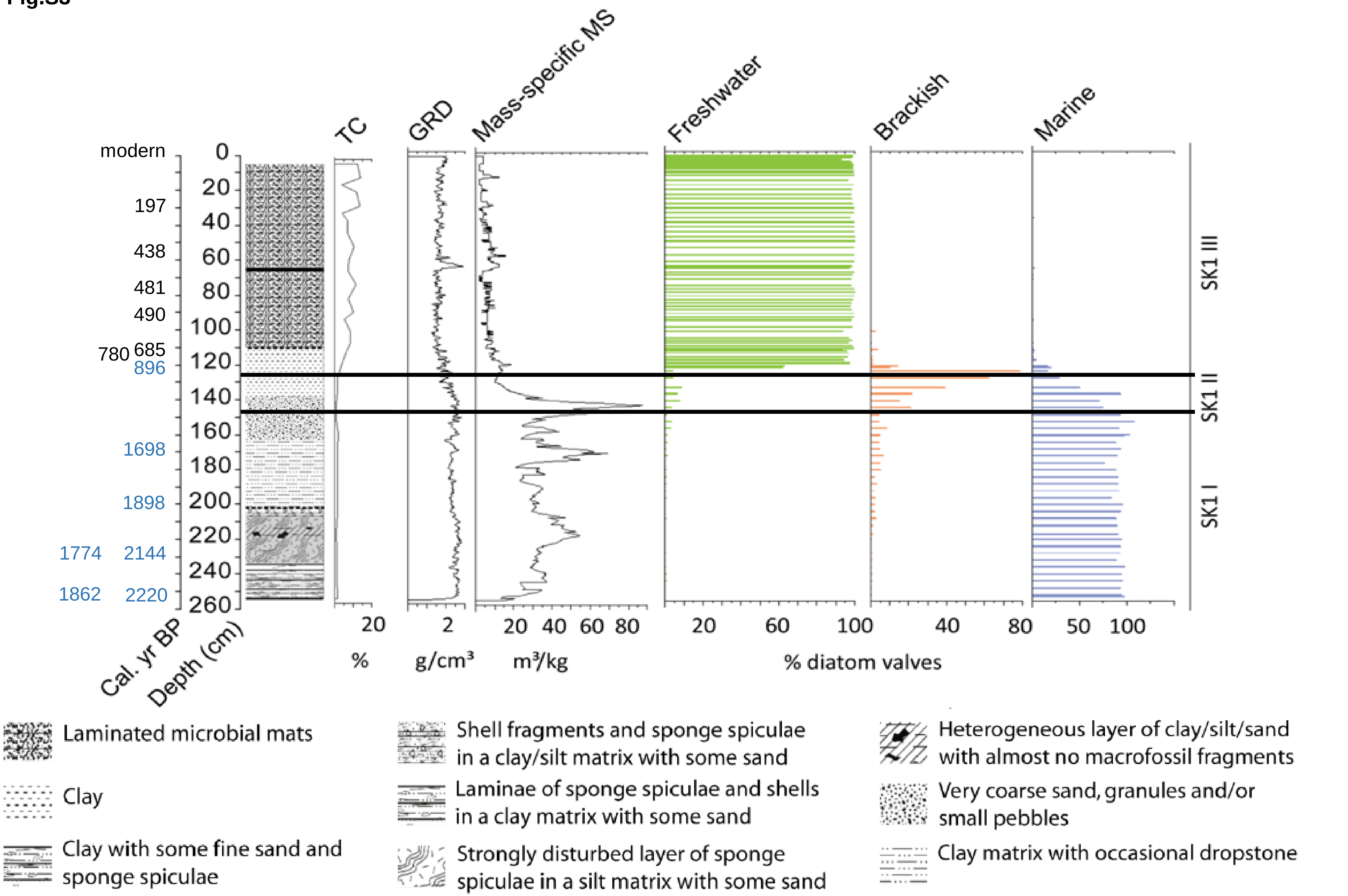

TC
GRD
Mass-specific MS
Freshwater
Brackish
Marine
modern
197
438
481
490
780 685
896
1698
1898
1774 2144
1862 2220
0
20
40
60
80
100
120
140
160
180
200
220
240
260
20
%
2
g/cm³
20 40 60 80
m³/kg
20 60 100
40 80
50 100
% diatom valves
SK1 III
SK1 II
SK1 I
Cal. yr BP
Depth (cm)
Laminated microbial mats
Clay
Clay with some fine sand and sponge spiculae
Shell fragments and sponge spiculae in a clay/silt matrix with some sand
Laminae of sponge spiculae and shells in a clay matrix with some sand
Strongly disturbed layer of sponge spiculae in a silt matrix with some sand
Heterogeneous layer of clay/silt/sand with almost no macrofossil fragments
Very coarse sand, granules and/or small pebbles
Clay matrix with occasional dropstone

Fig.S4

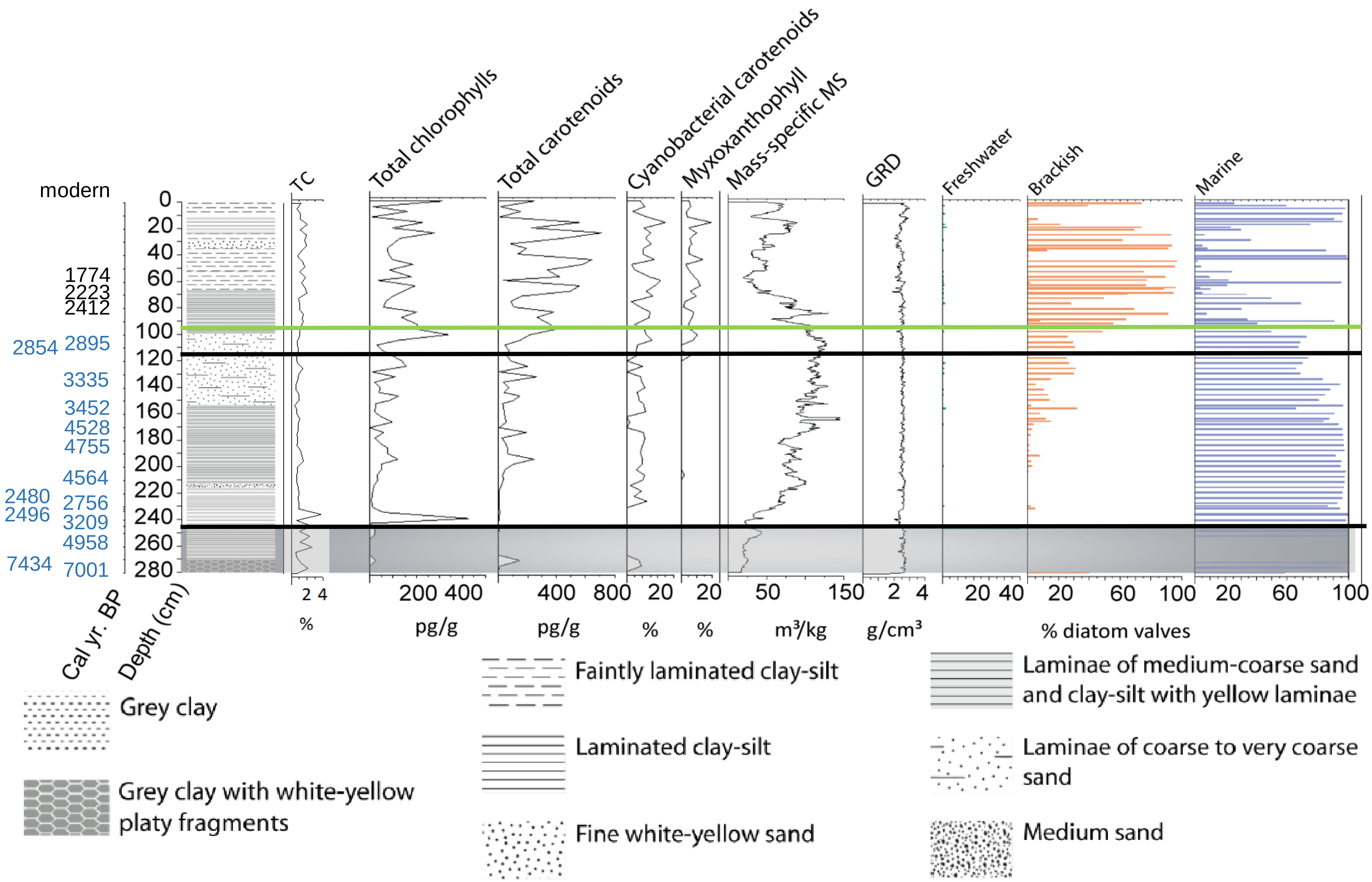

modern
TC
Total chlorophylls
Total carotenoids
Cyanobacterial carotenoids
Myxoxanthophyll
Mass-specific MS
GRD
Freshwater
Brackish
Marine
1774
2223
2412
2854 2895
3335
3452
4528
4755
4564
2480 2756
2496 3209
4958
7434 7001
SK4 III
SK4 II
SK4 I
%
pg/g
pg/g
%
%
m³/kg
g/cm³
% diatom valves
Cal yr. BP
Depth (cm)
Grey clay
Grey clay with white-yellow platy fragments
Faintly laminated clay-silt
Laminated clay-silt
Fine white-yellow sand
Laminae of medium-coarse sand and clay-silt with yellow laminae
Laminae of coarse to very coarse sand
Medium sand